

https://doi.org/10.1070/QEL16371

Optimisation of the prism coupling of optical whispering-gallery-mode microcavities

Yu.A. Demchenko, I.A. Bilenko, M.L. Gorodetsky

Abstract. **The methods for increasing the coupling efficiency of a prism with spheroidal microcavities, aimed at exciting whispering-gallery modes, have been analytically investigated. Optimal angles of incidence and incident beam parameters are obtained for a spheroidal cavity. The cavity eigenfrequency shift caused by the presence of a prism and the introduced loss by it is calculated.**

Keywords: *whispering-gallery-mode microcavities, prism coupling, coupling optimisation.*

1. Introduction

Optical whispering-gallery-mode (WGM) cavities [1, 2] are widely used in optics. Their Q factor can be as high as $\sim 10^{11}$ [3], which makes them promising for stabilising lasers [4]; designing detectors and sensors [5], optical filters [6], and modulators [7]; and generating optical combs [8]; they have also a great potential for quantum optomechanics [9].

Most of the methods used to implement coupling with these microcavities are based on the effect of an evanescent field: under conditions of total internal reflection in a cavity or a coupling element, there is a field outside, whose strength exponentially decreases when moving away from the reflecting surface. In this case, the longitudinal wave velocity is determined by the angle of incidence and can be varied to implement phase matching. The best cavity coupling (maximum extraction of incident power at the resonance frequency) was obtained using a tapered fibre; it reached 99.97% [10]. However, a stretched fibre is highly sensitive to mechanical vibrations and can easily be damaged. This problem can partially be solved by mounting a cavity with a fibre into a protected housing; however, the coupling efficiency of this scheme did not exceed 81% [11]. There are some other methods of coupling with WGM cavities, which are based on the application of polished fibres (coupling efficiency of about 10% [12]), fibres with a rubbed end face (pigtail fibres) [13] (coupling efficiency of ~60%), or different diffraction gratings (with a coupling efficiency up to 50% for gratings formed on the fibre end face [14] and up to 60% for gratings with a large period [15]). Historically, the use of a prism was the first method proposed for coupling with WGM cavities [16]. This method remains the simplest one; it provides a coupling efficiency up to 75% [17].

A prism is also used in many experiments [18–23] to implement coupling with cavities whose shape differs from spherical. The shape of these cavities can be approximated by a spheroid (ellipsoid of revolution), which, on the one hand, is a good approximation for describing the cavity shape in the light propagation region and, on the other hand, provides a high accuracy analytical approximation for eigenfrequencies [24].

In this study, we described the coupling between a prism and a cavity using an approach similar to that developed in [25]; it is based on calculating the diffraction in the far-field zone of the falling-out cavity field, tunnelling into the prism. The beam parameters in the prism that provide optimal coupling were investigated. The shift of the cavity eigenfrequencies was determined using an adiabatic invariant.

2. Mode field distribution outside the cavity

Necessary conditions for implementing coupling of radiation with a cavity through a prism are as follows: (i) the radiation must be focused on the inner surface of the prism at an angle exceeding the total internal reflection angle and (ii) the cavity must be located close to the focus [at a distance of $\sim\lambda/(2\pi)$, where λ is the light wavelength] [25]. As in the previous study [25], we chose a spherical coordinate system (ρ,θ,φ) with a centre coinciding with the cavity centre and a Cartesian coordinate system (x,y,z) with a centre located at the focus (Fig. 1). The angle between the z axis and the field wave vector in the prism and the angle between the x axis and the projection of the wave vector on the xy plane will be denoted as Θ and Φ, respectively.

Since the Helmholtz equation cannot be solved explicitly in the spheroidal geometry, we used the approximation [24] for the field distribution in the cavity. For the fundamental

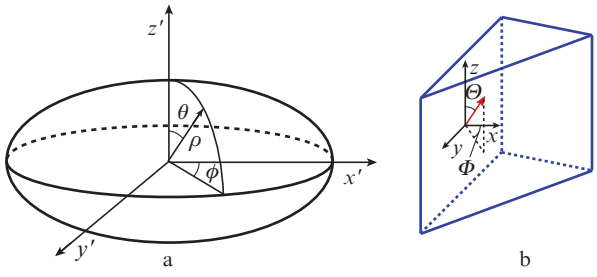

Figure 1. (a) Spherical coordinate system with an origin at the cavity centre and (b) Cartesian system with an origin at the focus.

Yu.A. Demchenko, I.A. Bilenko, M.L. Gorodetsky M.V. Lomonosov Moscow State University, Vorob'evy Gory, 119991 Moscow, Russia; e-mail: yury.demchenko@gmail.com

Received 18 March 2017; revision received 1 May 2017
Kvantovaya Elektronika **47** (8) 743–747 (2017)
Translated by Yu.P. Sin'kov

cavity mode, the angular field distribution on the cavity surface near the equator can be written as

$$E_{ll}(\rho = \alpha, \theta, \varphi) = c_{ll} \exp(-\tilde{\theta}^2/2) \exp(\mathrm{i}m\varphi). \quad (1)$$

For the high-order modes with $l - m \gg 1$, the field distribution can be written in the form

$$E_{lm}(\rho = \alpha, \theta, \varphi) = c_{lm}\left[\sqrt{2}\sqrt{l-m}\,\tilde{\theta} + \frac{\pi}{2}(l-m)\right]\exp(\mathrm{i}m\varphi), \quad (2)$$

where

$$\tilde{\theta} = \left(\frac{\pi}{2} - \theta\right)\sqrt[4]{\frac{m^2\tilde{b}^2}{\tilde{a}^2} - \frac{1}{4}};$$

$$\tilde{a} = a + Pr^*; \;\; \tilde{b} = \sqrt{\tilde{a}\left(\frac{b^2}{a} - \Delta_\rho\right)}; \quad (3)$$

$$\frac{1}{r^*} = k\sqrt{n_\mathrm{r}^2 - 1}; \;\; \Delta_\rho \approx 1.05 a m^{-2/3}$$

m is the azimuthal mode index; l is the angular mode index; n_r is the cavity refractive index; $P = 1$ and $P = 1/n_\mathrm{r}^2$ for TE and TM modes, respectively; $p = l - m$ is the meridional mode index; a and b are semiaxes of the spheroid, whose compression is defined as $c = (a - b)/a$; k is the wave propagation constant in vacuum; and c_{ll} and c_{lm} are normalisation constants. When calculating the effective geometric parameters of the spheroid, we disregarded the influence of the field falling out from the cavity, because the corresponding corrections are small in comparison with the initial parameters of the spheroid (on the order of $m^{-2/3}$); thus, it was assumed that $\tilde{a} \approx a$ and $\tilde{b} \approx b$.

Foreman et al. [26] studied the prism coupling using somewhat different field approximations, which were obtained in [27] based on the approximate solution of the scalar Helmholtz equation near the spheroid surface. However, we should note that the same expressions were previously obtained (using the same method) in monograph [2, p. 174], which was possibly unknown to the authors of [27]. The asymptotic equivalence of the distributions reported in [27] and [24] can easily be demonstrated using a simple coordinate transformation.

The method described in [27] and [2, p. 174] uses an orthogonal coordinate system, where the derivatives of the Lame coefficients are small and can be neglected; due to this, the Helmholtz equation can be simplified, and the solutions for the radial and angular parts can be written in terms of Airy and Hermite–Gauss functions, respectively. At the same time, an approximation for the radial part in terms of cylindrical Bessel functions was used in [24]. Since high-order Bessel functions can be approximated in terms of Airy functions, both approaches are asymptotically identical. When studying coupling, only angular distributions are of importance, and modes of very high orders are considered; therefore, the differences in the radial distribution approximations are insignificant. On the assumption that the spheroidal coordinates ζ and η correspond to the coordinates u (the distance from the point under consideration to the surface) and θ (the polar angle), the angular and radial parts of the field distribution can be presented as

$$E_\Theta(\theta, \varphi) = c_{ll} \exp\left(-\frac{\theta^2}{2\theta_m^2}\right) H\left(\frac{\theta}{\theta_m}\right) \exp(\mathrm{i}m\varphi),$$

$$E_\mathrm{R}(u) = Ai\left(\frac{u - \delta}{u_m}\right), \quad (4)$$

where H is a Hermite–Gauss function, Ai is an Airy function, and θ_m and δ are field distribution parameters in the cavity. It can easily be shown that the angular distribution for the fundamental and high-order modes can be obtained from (4) at $p = 0$ and $p \gg 1$, respectively.

The field outside the cavity decreases exponentially with a characteristic decay distance r^* [25]. The field decay outside a flattened cavity can be presented as $\exp[-z^2/(2a_z r^*) - y^2/(2a_y r^*)]$, where a_z and a_y are the radii of curvature of the cavity surface in the horizontal and meridional planes, respectively. In the case of an axisymmetric spheroidal cavity, the radius of curvature in the equatorial plane is $a_z = a$. In the meridional plane, the dependence of curvature on the angle θ is disregarded, and the radius is assumed to be equal to the radius of curvature at $\theta = 0$; correspondingly, $a_y = b^2/a$. Having multiplied the expressions for the field on the cavity surface, (1) and (2), with the derived expression for the field decay, one can obtain the field distribution on the prism surface. A Fresnel integral is used to pass from the field distribution on the prism surface to the field distribution within the prism. The field distribution is multiplied by $\exp[\mathrm{i}(k_z z + k_y y)]$ and integrated over the prism plane facing the cavity. The sizes of the region where the field penetrating from the cavity into the prism is not small are much smaller than the prism sizes; therefore, the integration can be performed in infinite limits. Under the assumption that $\tilde{k}_z = k_z/k$ and $\tilde{k}_y = k_y/k$, the integration result can be written as

$$E(k_z, k_y) \propto \exp\left[-\frac{(\tilde{k}_z - \tilde{k}_{z0})^2}{2\Delta\tilde{k}_z^2} - \frac{(\tilde{k}_y - \tilde{k}_{y0})^2}{2\Delta\tilde{k}_y^2}\right].$$

After the integration, one can find the $\tilde{k}_{z0}$ and $\tilde{k}_{y0}$ values determining the optimal angle of light incidence on the internal prism boundary and the characteristic widths of the ranges of optimal angles, $\Delta\tilde{k}_z^2$ and $\Delta\tilde{k}_y^2$, in the xz and xy planes, respectively. For $p = 0$,

$$\tilde{k}_{z0} = \cos\Theta = 0, \quad (5)$$

$$\Delta\tilde{k}_z^2 = \Delta\Theta^2 = \frac{rbm/a + a}{rb^2 n_\mathrm{p}^2 k^2} = \frac{mn_\mathrm{r}^2 a}{l^2 n_\mathrm{p}^2 b} + \frac{n_\mathrm{r} a^2}{l n_\mathrm{p}^2 b^2}\sqrt{n_\mathrm{r}^2 - 1}, \quad (6)$$

$$\tilde{k}_{y0} = \sin\Phi = \frac{m}{n_\mathrm{p} ka} \approx \frac{n_\mathrm{r}}{n_\mathrm{p}}, \quad (7)$$

$$\Delta\tilde{k}_y^2 = \Delta\Phi^2 \cos^2\Phi = \frac{1}{n_\mathrm{p}^2 k^2 ar} \approx \frac{n_\mathrm{r}\sqrt{n_\mathrm{r}^2 - 1}}{n_\mathrm{p}^2 l}, \quad (8)$$

and, for $p \gg 1$,

$$\tilde{k}_{z0} = \cos\Theta = \pm\frac{\sqrt{2bm}}{bn_\mathrm{p}k}\sqrt{\frac{l-m}{a}} \approx \pm\sqrt{2}\sqrt{\frac{a}{b}}\frac{n_\mathrm{r}}{n_\mathrm{p}}\frac{\sqrt{m(l-m)}}{l}, \quad (9)$$

$$\Delta\tilde{k}_z^2 = \Delta\Theta^2 \sin^2\Theta = \frac{a}{n_p^2 k^2 b^2 r} \approx \frac{a^2 n_r \sqrt{n_r^2 - 1}}{n_p^2 b^2 l}, \quad (10)$$

$$\tilde{k}_{y0} = \sin\Phi \sin\Theta = \frac{m}{n_p k a} \approx \frac{m n_r}{l n_p}, \quad (11)$$

$$\Delta\tilde{k}_y^2 = \Delta\Phi^2 \cos^2\Phi \sin^2\Theta = \frac{1}{n_p^2 k^2 a r} \approx \frac{n_r \sqrt{n_r^2 - 1}}{n_p^2 l}, \quad (12)$$

where n_p is the refractive index of the prism.

It can be seen that the contraction of the spheroid determines the field characteristics in the prism. One of the most important relations, $n_p > n_r$, which follows from the total internal reflection condition on the prism face and limits the choice of possible materials for the prism and cavity, can be obtained from (7) and (11). This condition does not change significantly with a change in b/a because of the rather weak dependence of the eigenfrequencies on the degree of cavity contraction [24]. The main difference from the case of an ideal sphere is the different field distribution in the vertical plane. For fundamental modes, the characteristic width of the field distribution in the prism increases with increasing degree of cavity contraction because of the reduction of the characteristic distribution width for the field penetrating from the cavity into the prism. For high-order modes (with $p \gg 1$), the dependence of the characteristic width on the degree of contraction is similar; it is determined mainly by the precession angle, which, in turn, depends on m/l [25]. Note that the field distributions near the cavity for the fundamental mode are described well by two-dimensional Gaussians; hence, the overlap integrals can easily be calculated in infinite limits.

The light propagation angles in the prism (Fig. 2) can be obtained from geometric optics formulas:

$$\Psi = \Phi - \alpha,$$

$$\beta = \arcsin[n_p \sin(\Phi - \alpha)],$$

$$\Delta\beta = \frac{n_p \cos(\Phi - \alpha)}{\sqrt{1 - n_p^2 \sin^2(\Phi - \alpha)}} \Delta\Phi.$$

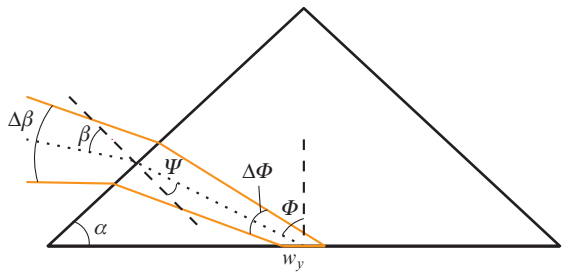

Figure 2. Ray trajectories in the prism.

3. Optimisation of the degree of coupling

Under the assumption that the beam $E_l(y,z)$ incident on a prism face has a Gaussian transverse field distribution and the angles in the prism are optimally fitted, one can obtain the degree of cavity contraction providing the highest degree coupling. We assume that the beam incident on the prism is focused on its surface and that the beam transverse sizes in the y and z directions near the focus are w_y and w, respectively; the w_y/w ratio depends on the angle of beam incidence.

To optimise the degree of coupling, we will maximise the overlap integral on the prism surface [28] between the cavity field $E_r(y,z)$ penetrating the prism and the radiation field:

$$l_{cs} \propto \frac{\int E_l(y,z) E_r(y,z)\,dy dz}{\sqrt{\int E_l^2(y,z)\,dy dz}\sqrt{\int E_r^2(y,z)\,dy dz}}$$

$$= \int \exp\left(-\frac{y^2}{w_y^2} - \frac{z^2}{w^2}\right) E_l(y,z)\,dy dz$$

$$\times \left[\sqrt{\int \exp\left(-2\frac{y^2}{w_y^2} - 2\frac{z^2}{w^2}\right) dy dz}\sqrt{\int E_l^2(y,z)\,dy dz}\right]^{-1}.$$

For the fundamental mode, the integral can be calculated and the result can be differentiated with respect to b/a to search for an extremum:

$$\frac{b}{a} = \frac{w^2}{4a^2} m + \frac{w}{2a}\sqrt[4]{\frac{n_r^2 - 1}{n_r^2}}\, m. \quad (13)$$

In the case of the fundamental mode, one can find analytically the root b/a of the equation, which is an extremum for the overlap integral. To make sure that this extremum is a maximum, we will take the second derivative of I_{cs} at this point. The expression for the second derivative at the extremum point is rather cumbersome; however, one can easily check that it is smaller than zero; this is an indication that the point under consideration is a maximum. The dependence of the optimal degree of contraction on the beam size w is presented in Fig. 3.

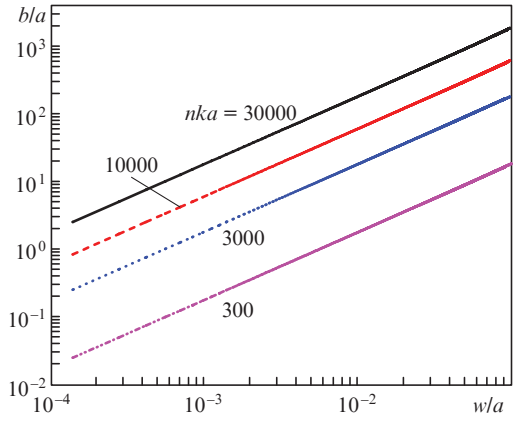

Figure 3. Parameters of a spheroid corresponding to its optimal shape at $n_r = 1.4$.

The excitation of modes with $p \gg 1$, which call for a Gaussian beam incident at some angle with respect to the xy plane [25], is not considered here. The optimal parameters do not depend simultaneously on w_y and w, because a cavity contraction changes significantly the field distribution only in the vertical plane. As can be seen in Fig. 4, the dependence of the degree of coupling on the cavity contraction is fairly weak.

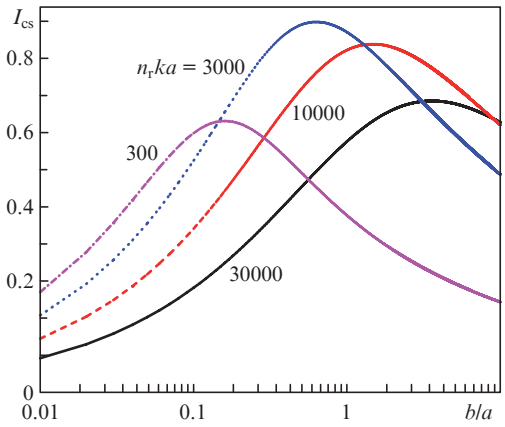

Figure 4. Dependences of the overlap integral on parameter b/a for fundamental modes at $a = 100$ μm, $n_r = 1.4$, $w = 1.41$ μm and $w_y = 2.83$ μm.

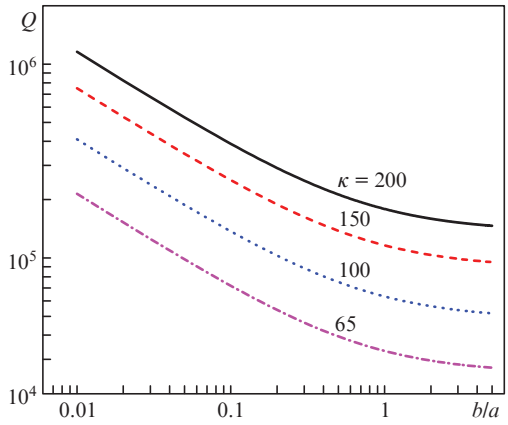

Figure 5. Dependences of the Q factor on parameter b/a at $n_r = 1.4$, $n_p = 1.5$ and $d = 0$; $\kappa = a/\lambda$.

For typical experimental values, the overlap integral changes only by 10% with a change in the degree of contraction by 30%.

The value of optimal cavity contraction found by us differs from that reported in [29], where it was suggested that the optimal coupling is obtained at equal ratios of the transverse beam sizes in the directions of the z and y axes for the initial laser beam and for the beam in the cavity on the prism face. The method proposed here is methodologically more correct, because the solution of coupled-mode equations [28] yields overlap integrals for the coupling coefficients; specifically these integrals are maximised in this study.

4. Loading Q factor

The presence of a coupling element (prism) results in the emission of energy from the cavity through this element. The energy loss on the emission through the prism can be characterised by the inverse value, which will be referred to as the loading Q factor. The cavity contraction also affects this parameter. It can be found from the formula relating the energy E accumulated in the cavity and the power P emitted through the prism:

$$Q = \frac{\omega E}{P}.$$

To find the power emitted into the prism, which is located at a distance d, we can integrate the energy density emerging from the cavity (here, as in the previous calculations, the prism surface is considered to be infinite). Thus, the loading Q factor has the form

$$Q = \frac{n_r^2}{n_p}\left[\frac{2\pi a(n_r^2-1)}{\lambda}\right]^{3/2}\exp\left(\frac{4\pi d\sqrt{n_r^2-1}}{\lambda}\right)$$

$$\times\sqrt{\frac{\pi}{\sqrt{n_r^2-1}}+\frac{\pi a}{bn_r}}.$$

This expression coincides with that for the Q factor of a sphere [25] at $a = b$ and changes with a change in the degree of cavity contraction (Fig. 5), which is related to the change in the shape of the area on the prism surface into which the field from the cavity efficiently penetrates. The loading Q factor, as in the case of a sphere, depends exponentially on the distance between the cavity and prism. Hence, one can easily implement optimal loading by choosing the necessary distance d.

5. Influence of the prism on the eigenfrequency shift and Q factor

Since the prism is located in the region where the cavity field rapidly decays with distance, its presence affects the cavity eigenfrequencies. The corresponding small frequency shift can easily be obtained using an adiabatic invariant as in [30]:

$$\frac{\Delta A}{E} = \frac{\Delta\omega}{\omega}.$$

Since the prism is sufficiently large, it can be considered as half-space. To find the work spent on the displacement of the prism from infinity to distance d, we will consider the difference in the energies in the presence of a prism at a distance d and in its absence. Under the assumption that the emerging cavity field E_r depends on only the distance d, we obtain

$$E_r(d) = -\int_d^\infty \mathrm{d}x\int|E(y,z)|^2\mathrm{d}S\exp\left(-\frac{2x}{r}\right)$$

$$= \frac{1}{2}\exp\left(-\frac{2d}{r}\right)\int|E(y,z)|^2\mathrm{d}S.$$

Thus, $\Delta A = E_r(d)(n_p^2-1)$ and

$$\frac{\Delta A}{E} = \frac{1}{Q}\frac{r/2}{c/\omega} = \frac{1}{Q}\frac{rk}{2} = \frac{1}{Q}\frac{n_p^2-1}{2\sqrt{n_r^2-1}}. \qquad (14)$$

In the presence of loss in the prism material, some part of energy from the cavity will be absorbed in it. Let us determine the contribution of this loss to the microcavity Q factor. To this end, we will substitute the complex refractive index of the prism material, $n_p = n_{pr} + in_{pi}$, into the expression for the Q factor:

$$Q_i = \frac{\omega_0}{2\delta} = \frac{1}{2\,\mathrm{Im}[\Delta A/E]}.$$

Let Q be equal to $Q = Q_0/n_\mathrm{p}$, where Q_0 is independent of n_p; then the imaginary part takes the form

$$\mathrm{Im}\left[\frac{\Delta A}{E}\right] = \frac{1}{Q_0\sqrt{n_\mathrm{r}^2-1}}\,\mathrm{Im}\left[\frac{n_\mathrm{p}^2-1}{n_\mathrm{p}}\right]$$

$$= \frac{1}{Q_0\sqrt{n_\mathrm{r}^2-1}}\,n_\mathrm{i}\left(\frac{1}{n_\mathrm{pi}^2+n_\mathrm{pr}^2}+1\right).$$

Substituting this expression for the imaginary part into the expression for the Q factor, we obtain

$$Q_\mathrm{i} = Q\sqrt{n_\mathrm{r}^2-1}\,\frac{n_\mathrm{pr}}{n_\mathrm{pi}}\,\frac{n_\mathrm{pr}^2+n_\mathrm{pi}^2}{n_\mathrm{pr}^2+n_\mathrm{pi}^2+1}. \qquad (15)$$

6. Conclusions

We have considered the influence of the contraction of a cavity on its coupling with a prism and on its loading Q factor. It was shown that the field distribution in the prism changes significantly with an increase in the degree of cavity contraction only along the contraction direction. Changing the cavity shape, one can make the requirements to the angle of inclination of the cavity with respect to the prism plane less stringent. The loading Q factor of a flattened cavity by a prism is found to depend weakly on the contraction. It is also shown that, having chosen the optimal parameters of the incident light, one can increase the degree of coupling between the cavity and prism by few percent.

Acknowledgements. This work was supported by the Ministry of Education and Science of the Russian Federation (Project No. RFMEFI585516X0005).

References

1. Braginsky V.B., Gorodetsky M.L., Ilchenko V.S. *Phys. Lett. A*, **137**, 393 (1989).
2. Gorodetsky M.L. *Opticheskie mikrorezonatory s gigantskoi dobrotnost'yu* (Optical Microresonators with A Giant Quality Factor) (Moscow: Fizmatlit, 2011).
3. Grudinin I., Ilchenko V., Maleki L. *Phys. Rev. A*, **74**, 063806 (2006).
4. Ilchenko V.S., Liang W., Maleki L., Matsko A.B., Savchenkov A.A., Seidel D. *Opt. Lett.*, **35**, 2822 (2010).
5. Foreman M.R., Swaim J.D., Vollmer F. *Adv. Opt. Photon.*, **7**, 168 (2015).
6. Ilchenko V.S., Maleki L., Matsko A.B., Savchenkov A.A. *IEEE Photon. Technol. Lett.*, **17**, 136 (2005).
7. Dalton L.R., Rabiei P., Steier W.H., Zhang C. *J. Lightwave Technol.*, **20**, 1968 (2002).
8. Del'Haye P., Gorodetsky M.L., Gavartin E., Herr T., Holzwarth R., Kippenberg T.J. *Phys. Rev. Lett.*, **107**, 63901 (2011).
9. Aspelmeyer M., Marquardt F., Kippenberg T.J. *Rev. Mod. Phys.*, **86**, 1391 (2014).
10. Kippenberg T.J., Painter O.J., Spillane S.M., Vahala K.J. *Phys. Rev. Lett.*, **94** (4), 043902 (2003).
11. Dong Y., Jin X., Wang K. *Appl. Opt.*, **54** (2), 277 (2015).
12. Dubreuil N., Hare J., Knight J.C. , Lefèvre V., Leventhal D.K., Sandoghdar V. *Opt. Lett.*, **20**, 813 (1995).
13. Iltchenko V., Maleki L., Yao S. *Simple Fiber-Optic Coupling for Microsphere Resonators* (NASA's Jet Propulsion Laboratory Tech Briefs, 2001).
14. Ding W., Gu B., Luan F., Yu X., Zhao C., Zhou Y. *Opt. Lett.*, **40**, 9 (2015).
15. Baldini F., Chiavaioli F., Farnesi D., Righini G.C., Soria S., Trono C., Conti G.N. *Opt. Express*, **23** (16), 21179 (2015).
16. Braginsky V.B., Gorodetsky M.L., Ilchenko V.S. *Phys. Lett. A*, **137** (7–8), 393 (1989).
17. Chang R.K., Pan Y. *Appl. Phys. Lett.*, **82** (4), 487 (2003).
18. Ilchenko V.S., Liang W., Maleki L., Matsko A.B., Savchenkov A.A., Seidel D. *Nature Photon.*, **5**, 293 (2011).
19. Becker P., Bohatý L., Breunig I., Josef U.F., Karsten B., Liebertz J. *Opt. Lett.*, **40**, 9 (2015).
20. Burkhart J., Ilchenko V.S., Liang W., Maleki L., Matsko A.B., McMillan J.F., Savchenkov A.A., Xie Z., Wong C.W. *Optica*, **2**, 1 (2015).
21. Fortsch M., Furst J.U., Leuchs G., Marquardt C., Schunk G., Schwefel H.G.L., Sedlmeir F., Strekalov D.V., Vogl U. *Opt. Express*, **22** (25), 30795 (2014).
22. Bennett A.M., Ilchenko V.S., Maleki L., Matsko A.B., Santini P., Savchenkov A.A. *Opt. Lett.*, **38**, 21 (2013).
23. Matsko A.B., Maleki L., Mohageg M. *Opt. Express*, **20** (15), 16704 (2012).
24. Demchenko Y.A., Gorodetsky M.L. *J. Opt. Soc. Am. B*, **30** (11), 3056 (2013).
25. Gorodetsky M.L., Ilchenko V.S. *Opt. Commun.*, **113**, 133 (1994).
26. Foreman M.R., Leuchs G., Schwefel H.G.L., Sedlmeir F. *J. Opt. Soc. Am. B*, **33** (11), 2177 (2016).
27. Buse K., Breunig I., Schwefel H.G.L., Sedlmeir F., Sturman B. *Opt. Express*, **21** (25), 30683 (2013).
28. Gorodetsky M.L., Ilchenko V.S., Savchenkov A.A. *Proc. SPIE*, **3267**, 251 (1998).
29. Abdalmalak K.A., Döhler G.H., García Muñoz L.E., Lampérez A.G., Malzer S., Preu S., Romano L.S., Santamaría-Botello G.A., Schwefel H.G.L., Sedlmeir F., Segovia-Vargas D., Weber H.B. *Opt. Express*, **24** (23), 26503 (2016).
30. Demchenko Yu.A., Gorodetsky M.L. V*estn. Mosk. Univ., Ser. 3: Fiz., Astron.*, (3), 32 (2015).